Journal of Physics: Condensed Matter

PAPER

Entropy driven incommensurate structures in the frustrated kagome staircase $Co_3V_2O_8$

To cite this article: Joel S Helton *et al* 2024 *J. Phys.: Condens. Matter* **36** 205801

View the article online for updates and enhancements.

You may also like

- Topological aspects of antiferromagnets
V Bonbien, Fengjun Zhuo, A Salimath et al.
- Role of isotropic and anisotropic Dzyaloshinskii–Moriya interaction on skyrmions, merons and antiskyrmions in the C_{nv} symmetric system
Sandip Bera
- Quantum interactions in topological R166 kagome magnet
Xitong Xu, Jia-Xin Yin, Zhe Qu et al.

This content was downloaded from IP address 129.6.123.192 on 20/02/2024 at 14:25

IOP Publishing Journal of Physics: Condensed Matter
J. Phys.: Condens. Matter **36** (2024) 205801 (14pp) https://doi.org/10.1088/1361-648X/ad266b

Entropy driven incommensurate structures in the frustrated kagome staircase $Co_3V_2O_8$

Joel S Helton[1,2,*], **Nyrissa Rogado**[3,4], **Robert J Cava**[3] and **Jeffrey W Lynn**[2]

[1] Department of Physics, United States Naval Academy, Annapolis, MD 21402, United States of America
[2] NIST Center for Neutron Research, National Institute of Standards and Technology, Gaithersburg, MD 20899, United States of America
[3] Department of Chemistry, Princeton University, Princeton, NJ 08544, United States of America

E-mail: helton@usna.edu

Received 25 August 2023, revised 27 October 2023
Accepted for publication 5 February 2024
Published 19 February 2024

Abstract

$Co_3V_2O_8$ features spin-3/2 moments arrayed on a kagome staircase lattice. A spin density wave with a continuously evolving propagation vector of $\vec{k} = (0, \delta, 0)$, showing both incommensurate states and multiple commensurate lock-ins, is observed at temperatures above the ferromagnetic ground state. Previous work has suggested that this changing propagation vector could be driven by changes in exchange interactions due to Co atom displacements. We present a straightforward model showing that a Hamiltonian with competing (but temperature independent) interactions can semi-quantitatively reproduce this behavior using a mean field approximation. The simulated spin density wave magnetic structures feature buckled kagome planes that are either ferromagnetically or antiferromagnetically ordered. Propagation vectors that differ from $\delta = 1/2$ will have multiple different ways of arranging these ferromagnetic layers that have very similar energies. This classical stacking entropy appears to be crucial in stabilizing the temperature-dependent propagation vector.

Keywords: entropy, frustrated magnetism, competing interactions, kagome staircase

1. Introduction

In frustrated spin systems the lattice geometry, disorder, or competing magnetic interactions yield a scenario in which no magnetically ordered structure can simultaneously satisfy every magnetic interaction [1, 2]. While the magnetic moments in $Co_3V_2O_8$ are arranged in a structure reminiscent of the highly frustrated kagome lattice, the frustration appears to arise primarily from competing interactions rather than the lattice geometry. The $M_3V_2O_8$ family of compounds (with M = Mn, Co, Ni, Cu, or Zn) display the kagome staircase structure, in which M^{2+} ions form buckled kagome planes of corner-sharing triangles that stack along the crystallographic b-axis. The edge-sharing MO_6 octahedra lead to M–O–M bond angles that are quite close to 90°, yielding nearest-neighbor superexchange interactions that are typically weak. Small differences in magnetocrystalline anisotropy and further-neighbor interactions can therefore yield very different ordered magnetic structures across this structurally similar family of materials. $Ni_3V_2O_8$ (with $S = 1$ Ni^{2+} ions) displays a complex magnetic phase diagram with several distinct spin density wave ordered structures [3]. The low-temperature incommensurate magnetic structure (observed between 4.0 K and 6.3 K at zero field) [4] is helical order that breaks inversion symmetry. $Ni_3V_2O_8$ is multiferroic, as this helical order is concomitant with ferroelectricity [5, 6] and a high-field reentrant ferroelectric phase is driven by an ordering under a magnetic field tilted away from the crystallographic axes

[4] Present address: DuPont Central Research and Development, Experimental Station, Wilmington, DE 19880.
[*] Author to whom any correspondence should be addressed.

© 2024 IOP Publishing Ltd

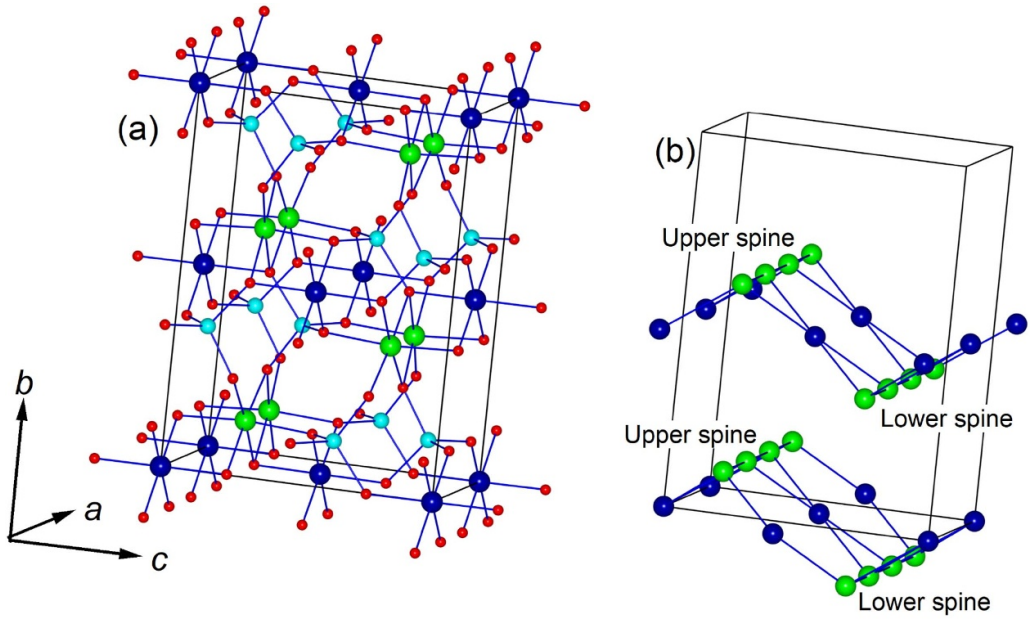

Figure 1. (a) Nuclear unit cell of $Co_3V_2O_8$. Co(1) cross-tie sites are shown in blue, Co(2) spine sites are shown in green, vanadium sites are shown in cyan, and oxygen sites are shown in red. (b) Two kagome layers of cobalt sites are shown, expanded beyond the first unit cell along the a direction. The first and second nearest-neighbor distances are shown to highlight the buckled kagome lattice structure. The cross-tie sites are located in the middle of a kagome layers Each layer contains an upper spine located above the cross-ties and a lower spine located below them. These crystal drawings were produced using VESTA [21].

[7]. Ferroelectricity has not been observed in $Co_3V_2O_8$ (with $S = 3/2$ Co^{2+} ions), but the vibrational mode leading to polarization in $Ni_3V_2O_8$ is magnetically sensitive and there is evidence of a magnetic field driven structural distortion [8, 9].

$Co_3V_2O_8$ also displays a complex magnetic phase diagram [10] with a transversely polarized spin density wave structure that displays alternating commensurate and incommensurate periodicities. All observed magnetic structures in $Co_3V_2O_8$ are Ising-like, with magnetic moments ordered along the crystallographic a-axis. The ground state, below $T_C = 6.2$ K, is ferromagnetic with an ordered moment of 2.73 μ_B on the spine sites and 1.54 μ_B on the cross-tie sites (see figure 1 for definition of the spine and cross-tie sites). There is evidence that the moment missing from the cross-tie sites may reside on the V^{5+} and O^{2-} ions [11]. Between T_C and $T_N = 11.3$ K there is a transversely polarized spin density wave structure with a propagation vector of $\vec{k} = (0, \delta, 0)$ along the b-axis. There are distinct commensurate lock-in phases at $\delta = 1/3$ (T_C to 6.5 K) and $\delta = 1/2$ (6.9 K–8.6 K) interspersed with incommensurate values of δ [10]. The application of modest magnetic fields along the a-axis (the magnetization easy axis) leads to a new commensurate lock-in phase with $\delta = 2/5$ [12]. Complicated magnetic phase diagrams are also observed with magnetic fields applied along the b-axis [13] or c-axis [14]. The spin density wave peaks with propagation vectors other than $\delta = 1/2$ were found to be broad [15]. This material shows an unusually large change in thermal conductivity with applied magnetic field [16] due to critical spin fluctuations scattering phonons near phase transitions; this indicates possible use as a heat valve. Spin waves in the ferromagnetic ground state display a spin gap of about 1.5 meV and a bandwidth of about 1 meV for excitations within the ac-plane [17] and along the b-axis [13]. Well-defined spin waves were not observed in the $\delta = 1/2$ spin density wave phase, with the inelastic spectral weight found in broad peaks of diffuse scattering centered at antiferromagnetic positions. An analysis of the spin wave excitations in the ferromagnetic ground state required five distinct superexchange interactions, distinct single-ion anisotropies on the two lattice sites, and a significant Dzyaloshinskii-Moriya interaction [18] to fully explain the spectra.

A full accounting of the relevant magnetic interactions in $Co_3V_2O_8$ is a daunting task given the two crystallographically distinct spin sites, the likely presence of significant moment on V^{5+} and O^{2-} ions [11], significant magnetocrystalline anisotropy [19], and the possibility of changing interaction strengths due to Co displacements [8]. Despite these complications we will show that a model consisting of the Hamiltonian previously used to describe the spin waves [18] plus two interplanar antiferromagnetic interactions suggested by a minimal Ising model [10] reproduces many of the observed features of the magnetic phase diagram. In this model the temperature evolution of the propagation vector does not require any change in coupling strengths but is driven by thermal fluctuations related to the entropy of stacking ferromagnetic and antiferromagnetic layers in patterns with nearly equivalent energies.

2. Methods

$Co_3V_2O_8$ crystallizes in the orthorhombic *Cmca* space group with lattice parameters at $T = 12.5$ K of $a = 6.027$ Å,

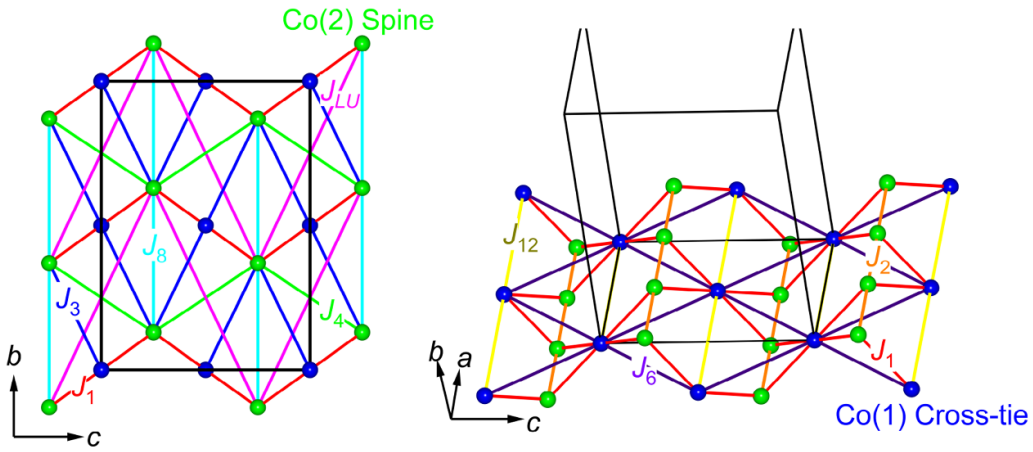

Figure 2. Magnetic couplings considered in the simulation. Co(1) cross-tie sites are shown in blue while Co(2) spine sites are shown in green. Co–O–Co superexchange pathways J_1 (red) and J_2 (orange) are shown as well as Co–O–V–O–Co pathways J_3 (blue), J_4 (green), J_6 (purple), J_8 (cyan), and J_{12} (yellow). J_{LU} (magenta) was suggested by a minimal Ising model [10].

$b = 11.483$ Å, and $c = 8.296$ Å [10, 20]. The nuclear unit cell is displayed in figure 1. This structure has two crystallographically inequivalent Co sites, with the Co(1) sites (at the 4*a* Wyckoff positions) referred to as the 'cross-ties' and the Co(2) sites (at the 8*e* Wyckoff positions) referred to as the 'spines'. The Co(2) spine sites form chains running along the *a*-axis. The cross-tie sites sit in the middle of the buckled kagome layers (at $y = 0$ or $y = b/2$). In a given kagome layer, half of the Co(2) sites will be on an upper spine above the cross-ties (at $y \approx 0.13b$ or $y \approx 0.63b$) while the other half will be on a lower spine (at $y \approx -0.13b$ or $y \approx 0.37b$). There are two possible pathways for Co–O–Co superexchange. The nearest-neighbor interaction, J_1, is 2.966 Å between a spine site and an adjacent cross-tie site. The second nearest-neighbor interaction, J_2, is 3.014 Å between adjacent spine sites. Both of these interactions are within the same buckled kagome plane. Given that the spin density wave structures feature a propagation vector parallel to the *b*-axis [10] and that the spin wave bandwidth along the $[0K0]$ direction is comparable to that within the $[H0L]$ plane [18] it is clear that there must be significant magnetic coupling between the buckled kagome planes and that it is therefore necessary to consider further-neighbor interactions. If we expand our scope to Co–O–V–O–Co pathways there are six additional possible interactions to consider; while these can entail fairly large distances there is evidence that a significant amount of magnetic moment may reside on the V^{5+} and O^{2-} ions [11] making such interaction pathways plausible. The third nearest-neighbor interaction, J_3, is 4.963 Å between a spine site on one layer and a cross-tie site on the next layer. The fourth nearest-neighbor interaction, J_4, is 4.981 Å between a spine site on one layer and a spine site on the next layer. The fifth nearest-neighbor interaction, J_5, is 5.109 Å between sites on the lower spine and upper spine of the same layer. The eighth nearest-neighbor interaction, J_8, is 5.742 Å between a spine site on one layer and a spine site directly above it along the *b*-axis. The sixth nearest-neighbor (J_6, 5.127 Å) and twelfth nearest-neighbor (J_{12}, 6.027 Å) interactions are between cross-tie sites in the same buckled kagome plane. (There are several other Co–Co distances smaller than the twelfth nearest-neighbor, but they are not considered due to the lack of a Co–O–V–O–Co pathway.) A minimal Ising model [10] argued that the observed propagation vector required a nonzero coupling J_{LU} between a spin on the lower spine of one kagome plane and a spin on the upper spine of the next higher kagome plane. These possible couplings are shown in figure 2. Spin wave measurements [18] were modeled with $J_2 = J_5 = 0$, so J_5 is excluded from the figure. The minimal Ising model in Chen *et al* [10] also considered a temperature-dependent effective interaction between the upper and lower spines on the same kagome layer (referred to as J_3 in that work but corresponding to the fifth nearest-neighbor Co–Co distance). This effective spine-spine interaction acted through the intermediate cross-tie site and was temperature-dependent due to the changing ordered moment of the cross-tie spins. By considering cross-tie sites in addition to the spines, this work fully captures this interaction with only a temperature-independent J_1.

Neutron single crystal diffraction measurements were performed on the BT-4 thermal triple axis spectrometer at the NIST Center for Neutron Research using a 14.7 meV neutron energy. A small ($\approx 3 \times 3 \times 2\,\mathrm{mm}^3$), high-quality single crystal sample that had previously been used for single crystal diffraction [10, 12], including the initial identification of the $\delta = 1/3$ phase, was aligned in the $[HK0]$ scattering plane. The sample was cooled in a closed cycle refrigerator to a set point of $T = 6$ K; this is slightly below the literature transition temperature of $T_C = 6.2$ K, but peaks with a propagation vector of $\delta = 1/3$ were clearly observed. Measurements were also performed at $T = 3$ K, in the ferromagnetic phase, and at $T = 15$ K in the paramagnetic phase. An 80′ collimator and a pyrolytic graphite filter were placed both between the monochromator and the sample and between the sample and the analyzer, and an 80′ collimator was placed between the analyzer and the detector. Both θ scan rocking curves and $\theta - 2\theta$ curves were measured for 21 reciprocal space positions in the $[HK0]$ scattering plane. At $T = 6$ K intensity was

observed at $[H, K, 0]$ positions where H was an even integer and K was an even integer $\pm 1/3$; for example, the greatest intensity was observed at $[2,\ 4.33,\ 0]$. The higher-order peaks were observed as intensity at positions where H was an even integer and K was an odd integer, such as $[0,\ 1,\ 0]$. The integrated intensities of peaks through the θ scan rocking curves were determined and corrected for the resolution ellipsoid. The intensities were normalized by comparing to both nuclear peaks measured at $T = 15\,\mathrm{K}$ and ferromagnetic peaks measured at $T = 3\,\mathrm{K}$; for comparison to ferromagnetic peaks we used the magnetic structure reported by Chen *et al* [10]

3. Theory

Our Hamiltonian is

$$\hat{\mathcal{H}} = \sum_{<i,j>} J_{ij}\vec{S}_i \cdot \vec{S}_j + \sum_{i,\mu} A_{i,\mu}\left(S_{i,\mu}\right)^2 + \sum_{<i,j>} \vec{D}_{ij} \cdot \left(\vec{S}_i \times \vec{S}_j\right) - g\mu_B \sum_i \vec{S}_i \cdot \mu_0 \vec{H}_{\mathrm{ext}} \quad (1)$$

where the summation $<i,j>$ is over pairs of spins, J_{ij} is the Heisenberg exchange term between spins i and j, $A_{i,\mu}$ is the μ-component ($\mu = x,\ y,\ z$) of the single-ion anisotropy parameter for spin i, $\vec{D}_{ij}$ is the Dzyaloshinskii–Moriya anisotropic exchange term between spins i and j, and $\vec{H}_{\mathrm{ext}}$ is the external applied magnetic field.

We follow the molecular field theory of Weiss [22] and assume that the effects of the first three terms in the Hamiltonian can be reproduced by a molecular field at each spin site that adds to the external applied magnetic field. This yields a total effective magnetic field at site i given by

$$\mu_0 \vec{H}_{\mathrm{eff},i} = -\sum_j \frac{J_{ij}}{g\mu_B}\vec{S}_j - \sum_\mu \frac{2A_{i,\mu}S_{i,\mu}\hat{\mu}}{g\mu_B} - \sum_j \frac{\left(\vec{S}_j \times \vec{D}_{ij}\right)}{g\mu_B} + \mu_0 \vec{H}_{\mathrm{ext}} \quad (2)$$

and a self-consistent solution is a magnetic structure where the ordered moment at site i is given by

$$g\mu_B \vec{S}_i = g\mu_B S B_J\left(S\frac{g\mu_B\mu_0 H_{\mathrm{eff},i}}{k_B T}\right)\hat{H}_{\mathrm{eff},i} \quad (3)$$

where $B_J(x)$ is the Brillouin function and S is the spin size.

The experimentally observed magnetic structure of $Co_3V_2O_8$ in its $\delta = 1/2$ phase [10] features alternating ferromagnetic and antiferromagnetic kagome layers. In the ferromagnetic layers all spins are aligned to point in the same direction; the spine and cross-tie sites have respective ordered moments of $1.39\,\mu_B$ and $1.17\,\mu_B$. In antiferromagnetic layers the upper and lower spines feature spins with an ordered moment of $2.55\,\mu_B$ that are aligned in opposite directions, and there is no ordered moment on the frustrated cross-ties. This ordered structure is displayed in figure 3(a). At the bottom of the magnetic unit cell is an antiferromagnetic layer in which the lower spine spins are ordered along the $-a$ direction while the upper spine spins are ordered along the $+a$ direction. This is followed by a ferromagnetic layer with all spins pointing along the $+a$ direction, then an antiferromagnetic layer where the lower spine is ordered along the $+a$ direction and the upper spine is ordered along the $-a$ directions, and finally a ferromagnetic layer ordered along the $-a$ direction. This motif of ferromagnetic and antiferromagnetic layers can be extended to a different periodicity by including more than one adjacent ferromagnetic layer between antiferromagnetic layers. Figure 3(b) shows an ordered structure with a second ferromagnetic layer pointing along the $+a$ direction but still only one ferromagnetic layer pointing along the $-a$ direction. This structure is ferrimagnetic, with a net magnetic moment pointing along the $+a$ direction. This simulated magnetic structure is likely similar to the commensurate lock-in with $\delta = 2/5$ that was observed in applied magnetic fields [12]. Figure 3(c) displays a $\delta = 1/3$ structure with two ferromagnetic layers between each antiferromagnetic layer.

Generally, a magnetic structure following this motif of ferromagnetic and antiferromagnetic layers can be described by a propagation vector component δ which is equal to the fraction of kagome layers that are antiferromagnetic layers. We will first consider a magnetic structure consisting of ferromagnetic and antiferromagnetic layers where all spine sites have the same ordered moment (S_s) and all cross-tie sites in ferromagnetic layers have the same moment (S_c) while cross-tie sites in antiferromagnetic layers are fully frustrated and have no ordered moment: the energy of this magnetic structure using the given Hamiltonian will depend upon the number of antiferromagnetic layers (and therefore on δ) but, so long as two antiferromagnetic layers are never adjacent, the energy does not depend upon the location of the antiferromagnetic layers. This implies that spin density wave ordered structures with a δ less than $1/2$ will feature large degeneracies. Placing two antiferromagnetic layers adjacent to one another is energetically unfavorable, provided that J_{LU} is nonzero and antiferromagnetic. The energy per unit cell of such a structure with $\delta \leqslant 1/2$ that never has two antiferromagnetic layers adjacent to one another is given by

$$\begin{aligned} E(\delta) = {} & 16\left[(1-\delta)(J_1+J_3)\right]S_sS_c \\ & + 8\left[J_2 + J_4 + (1-2\delta)(J_5+J_8) + (1-4\delta)J_{LU}\right]S_s^2 \\ & + 4\left[(1-\delta)(2J_6+J_{12})\right]S_c^2. \end{aligned}$$

If $4(J_1+J_3)S_sS_c + 4(J_5+J_8+2J_{LU})S_s^2 + (2J_6+J_{12})S_c^2 = 0$ then $\dfrac{\mathrm{d}E}{\mathrm{d}\delta} = 0$ and the energy of different ordered structures is independent of δ. Using the Hamiltonian values given in the supplementary information of [18] this will occur so long as $J_8 + 2J_{LU} \approx 0.3\,\mathrm{meV}$. When $J_8 + 2J_{LU}$ is slightly smaller than this value we would expect a ferromagnetic ground state, but at higher temperatures thermal fluctuations could select spin density waves with a range of commensurate or incommensurate propagation vectors.

Magnetic structures are determined by simulating 720 Co spins in a structure that is 60 unit cells stacked along the b-axis

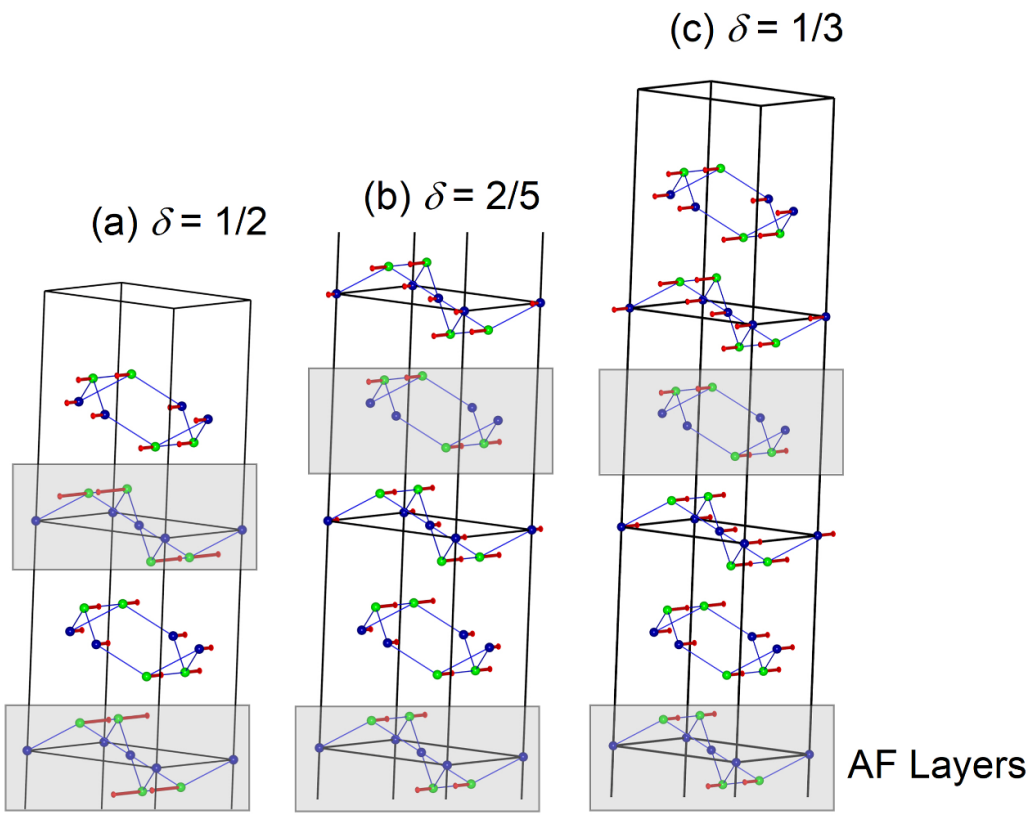

Figure 3. Example magnetic structures. Antiferromagnetic layers, in which the cross-tie sites are fully frustrated with no order moment and Co ions on the upper and lower spines are ordered in opposite directions, are highlighted by semitransparent gray boxes. (a) One magnetic unit cell (two nuclear unit cells) for the $\delta = 1/2$ ordered structure. Moment sizes represent the refined values from Chen *et al* [10] performed at 8.4 K. (b) One effective magnetic unit cell (2.5 nuclear unit cells) of a ferrimagnetic ordered structure with $\delta = 2/5$. (Given the *AB* stacking of the kagome layers, the actual magnetic unit cell is twice this large.) The moment sizes represent simulated values at 9.5 K and 0.15 T from this work, doubled in scale relative to the other two panels of this figure. (c) One magnetic unit cell (three nuclear unit cells) for the $\delta = 1/3$ ordered structures. Moment sizes represent the refined structure for data measured at 6.0 K and reported in this work.

(with no enlargement along the *a*-axis or *c*-axis) and periodic boundary conditions. 245 initial spin structures are chosen to reflect likely magnetic orderings. For each initial spin structure the molecular field process described above is applied until a self-consistent magnetic order is reached. The model Hamiltonian is used to determine the molecular field at a single Co site. The spin value at that site is changed to match the value given by the Brillouin function using an effective magnetic field that is the molecular field added to any external magnetic field. This is performed for each spin site in turn and is repeated until a self-consistent solution is obtained. The free energy is determined, with the entropy calculated as described in the appendix. This is then repeated for each of the 245 initial spin structures, and the self-consistent solution with the lowest free energy is taken as the simulated magnetic structure. 203 of these initial spin structures are identical during every run of the simulation; they represent spin structures built from our motif of alternating ferromagnetic and antiferromagnetic layers with all possible δ values from 0 to 1 in steps of 1/60 in patterns that feature no net magnetic moment and in patterns intended to maximize the net magnetic moment. 40 additional initial structures are chosen for each run of the simulation, intended to ensure that structures differing from our motif are not missed. For much smaller systems (no more than six stacked unit cells, as opposed to the 60 in our simulation) it is computationally feasible to find the lowest free energy structure by this method with initial spin structures chosen by assigning random spin directions. Systems consisting of two through six stacked unit cells are considered in this way. The lowest free energy state for these reduced systems is found and repeated between five and 30 times to build a 60 unit cell system that serves as initial spin structure. Finally, the last two initial spin structures are determined by slightly perturbing the lowest free energy state up to that point in a way that maximizes the effect of the Dzyaloshinskii-Moriya interaction. These final 42 initial spin structures are always included to avoid biasing results toward our expected structural motif, but every run of the simulation with the model Hamiltonian has returned a lowest free energy magnetic structure that matches the expected motif.

4. Results

Magnetic structures were simulated with the spin sizes and Hamiltonian from the supplementary materials of [18], which were determined from spin wave modeling with reduced

Table 1. Spin Hamiltonian parameters used for the simulations. All values except J_8 and J_{LU} were taken from the supplementary information of [18]. Single ion anisotropy values are set to zero along the easy axis. $J<0$ are ferromagnetic while $J>0$ are antiferromagnetic.

S_c	0.770	J_8	0.140 meV
S_s	1.365	J_{LU}	0.038 meV
J_1	−0.320 meV	$A_{c,x}$	0.850 meV
J_3	−0.250 meV	$A_{c,y}$	1.240 meV
J_4	−0.250 meV	$A_{s,y}$	1.770 meV
J_6	0.020 meV	$A_{s,z}$	1.120 meV
J_{12}	0.044 meV	$D_{1,x}$	0.210 meV

cobalt spins of $S_c = 0.770$ for cross-ties and $S_s = 1.365$ for spines. The single ion anisotropy parameters have been shifted so that the component along the easy axis (the a-axis for spines and the c-axis for cross-ties) is set to zero. $J_8 = 0.140$ meV and $J_{LU} = 0.038$ meV were added to provide a semi-quantitative match to the experimentally observed [10] evolution of the propagation vector in zero applied field. An antiferromagnetic exchange along J_8 with a strength about one third of this had been suggested in $Ni_3V_2O_8$ [4]. The spin wave modeling using SpinW [23] reported in [18] was repeated with these two additional antiferromagnetic couplings included and it was confirmed that these two terms do not perceptibly change the spin wave spectrum (spin wave positions are unchanged to a sensitivity of at least 0.01 meV). This confirms that the simulated Hamiltonian is consistent with measured spin waves in the ferromagnetic phase. The complete set of parameters is listed in table 1. The entropy per kagome layer of a given ordered structure was determined using equations (15) and (20) derived in the appendix.

When calculating free energies, the energy scales with the number of spins while the stacking entropy scales with the number of buckled kagome layers along the b-axis; increasing the size of the considered system within the ac-plane will cause the energy to increase, but not the stacking entropy. The simulation does not enlarge the unit cell within the ac-plane, so that energy per unit cell in the ac-plane is calculated. This needs to be compared with the entropy per unit cell in the ac-plane, determined by diving the overall entropy by the number of ac-plane unit cells in the system. The simulation achieved this by multiplying the overall calculated entropy by a scale factor; this scale factor can be thought of as the inverse of the number of unit cells in the ac-plane. This scale factor was an adjustable parameter, and a value of 0.0035 was chosen to best match the measured diffraction results. This scale factor corresponds to 290 unit cells in the ac-plane, which could be achieved by domains with an average diameter of 135 Å in the ac-plane. A correlation length of 220 Å had been found [15] along the b-axis at a temperature where $\delta \approx 0.4$, so a 135 Å domain size in the ac-plane is reasonable.

Figure 4 displays the scattering intensity for the simulated magnetic structures as a function of temperature. The simulation determined the lowest free energy structure at each temperature (with step of 0.05 K). The calculated neutron scattering intensity for each structure was determined and then convolved with a Gaussian with a width (standard deviation) of 0.02 r.l.u. to mimic an instrumental resolution. These Hamiltonian parameters reproduce the experimentally observed data quite well. Ferromagnetism gives way to a spin density wave at 6.0 K which locks in to a $\delta = 1/3$ propagation vector between 6.5 K and 7.0 K. This is followed by incommensurate structures with a steadily evolving δ up to 8.3 K. In this region a weak higher-order reflection is present at $\delta' = 2 - 3\delta$, just as was experimentally observed [10]. The $\delta = 1/2$ lock-in occurs from 8.3 K to about 11.0 K. Experimentally, incommensurate structures with $1/2 < \delta < 0.55$ were observed at temperatures a bit below T_N; in our simulation no magnetic structure with $\delta > 1/2$ is ever observed to minimize the free energy. While these states do have a higher entropy than the $\delta = 1/2$ lock-in they do not have a higher entropy than states with δ values a bit below $1/2$. Some other mechanism (perhaps a breakdown of the pattern of alternating ferromagnetic and antiferromagnetic layers) is needed to account for these states.

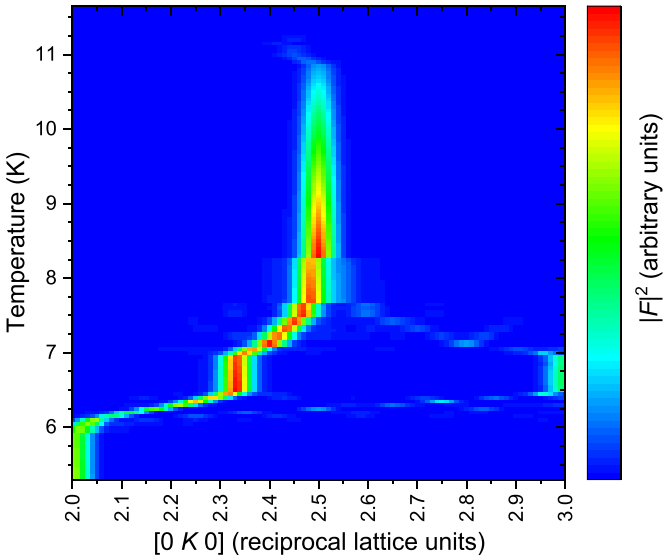

Figure 4. Simulated neutron scattering intensity (the norm-square of the structure factor) for the model Hamiltonian as a function of temperature.

At $T = 8.4$ K the simulation finds that the lowest free energy self-consistent solution for this Hamiltonian is one with $\delta = 1/2$. Figure 5 displays the ordered moment along the a-axis across two unit cells for both this simulation and the results of powder neutron diffraction measurements at this temperature from [10]. The ordered moment in the simulated results is fully along the a-axis, with no components along the other axes. The simulated results follow the experimental refinement with alternating ferromagnetic and antiferromagnetic layers and have very similar cross-tie ordered moments. Powder diffraction measurements found a significantly larger ordered moment of the antiferromagnetic layer spine sites than on the

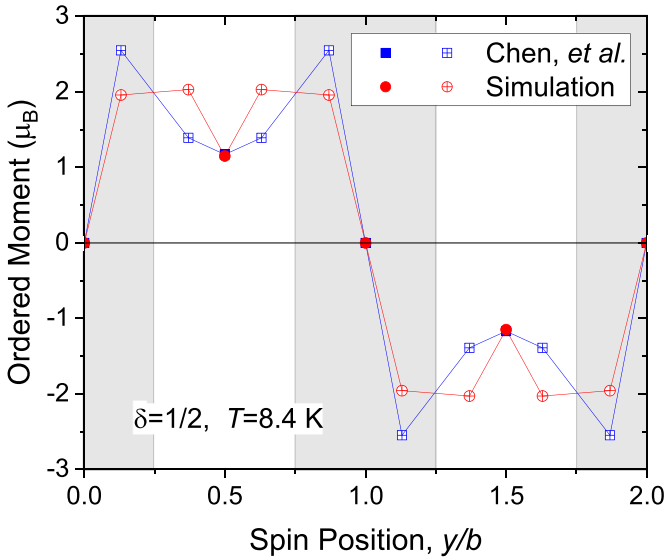

Figure 5. Ordered moment along the a-axis for the $\delta = 1/2$ phase at $T = 8.4$ K. Results are shown for the refinement of neutron powder diffraction data from Chen *et al* [10] and from the simulated results. Cross-tie sites are shown as solid symbols, while spine sites are shown as hollow symbols with perpendicular lines. Antiferromagnetic layers are highlighted by semitransparent gray boxes.

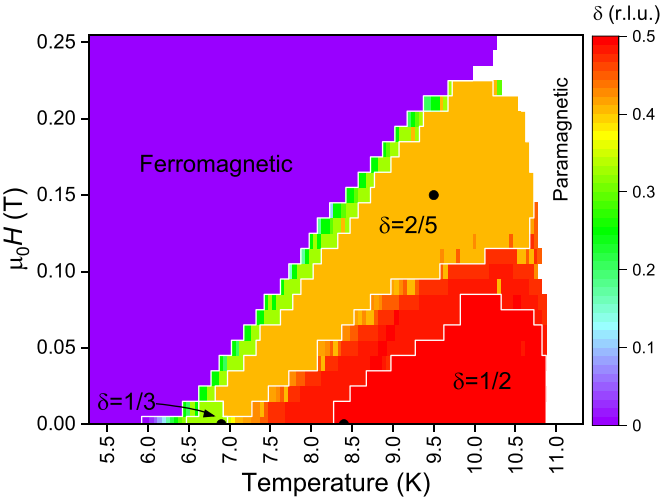

Figure 6. *HT* phase diagram for simulated structures using the considered Hamiltonian with magnetic fields applied along the a-axis. The color scale is used to display δ, where the propagation vector is $\vec{k} = (0, \delta, 0)$. Boundaries of the commensurate lock-ins are shown with white lines. The three black dots refer to the places in the phase diagram where the simulated structures shown in figures 3(b), 5 and 7(a) were determined.

ferromagnetic layer spin sites, which is not reflected in the simulated data.

Figure 6 shows the simulated *HT* phase diagram for this Hamiltonian and with magnetic fields along the a-axis (the magnetization easy-axis). As is observed experimentally from single crystal neutron diffraction [12] very small applied fields destabilize the $\delta = 1/3$ commensurate lock-in and produce a $\delta = 2/5$ commensurate lock-in. This $\delta = 2/5$ phase in the simulation results consists of sets of two ferromagnetic layers pointing along the field direction and single ferromagnetic layers pointing opposite the field direction separated by antiferromagnetic layers, providing a net ferrimagnetic moment along the a-axis. However, the applied field needed to suppress spin density wave order in the simulation is almost a factor of two smaller than the experimentally observed value and the shape of the $\delta = 1/2$ lock-in differs from the experimental phase diagram. Still, this strongly suggests that the $\delta = 2/5$ commensurate lock-in observed experimentally features the same motif of alternating ferromagnetic and antiferromagnetic layers.

The integrated intensities of 13 magnetic reflections at $T = 6$ K in the $\delta = 1/3$ phase were measured using neutron single crystal diffraction. The calculated intensities for these reflections were determined for a structure consisting of two ferromagnetic layers between each antiferromagnetic layer. These calculated intensities were fit to the measured intensities with four fit parameters: the ordered moments for ferromagnetic layer cross-ties, the antiferromagnetic layer spines, and both the upper and lower spines on ferromagnetic layers. The best fit matched the measured intensities fairly well, but produced a cross-tie ordered moment of $1.87(2)\,\mu_B$. Given that even in the ferromagnetic phase the cross-tie ordered moment is only $1.54\,\mu_B$ the fit was repeated with this as the maximum possible cross-tie ordered moment. This fit did not match the data quite as well, but captured the intensities of the strongest magnetic reflections reasonably well. These results are displayed in figure 7. Panel (a) shows the ordered moments for both the refined structure determined by fitting the diffraction data and from the simulation in the $\delta = 1/3$ phase. Both display the same motif of two consecutive ferromagnetic layers followed by an antiferromagnetic layer. The simulated structure has significantly larger ordered moments on the spine sites. Panel (b) compares the calculated intensity of magnetic reflections for the moments displayed in panel (a) to the measured intensity of the magnetic reflections. The motif of two ferromagnetic layers followed by an antiferromagnetic layer is consistent with the measured intensities in this phase. Some of the difference between the measured and calculated intensities could be due to the fact that this simulation models purely magnetic peaks at these positions while polarized diffraction data [10] found a modest intensity in the non-spin-flip channel that indicated a subtle structural distortion.

5. Discussion

A single crystal neutron diffraction study of $Co_3V_2O_8$ [15] found that the reflection in the $\delta = 1/2$ phase was resolution limited. However, the reflections in both the $\delta = 1/3$ phase and the incommensurate phase with $\delta > 1/2$ featured a broad Lorentzian component on top of a dominant resolution limited peak. The reflection at a temperature with an incommensurate propagation vector of $\delta \approx 0.4$ was purely a Lorentzian with a width (FWHM) of 0.015 r.l.u. A single crystal spectroscopy study [18] did not find well-defined spin waves in the

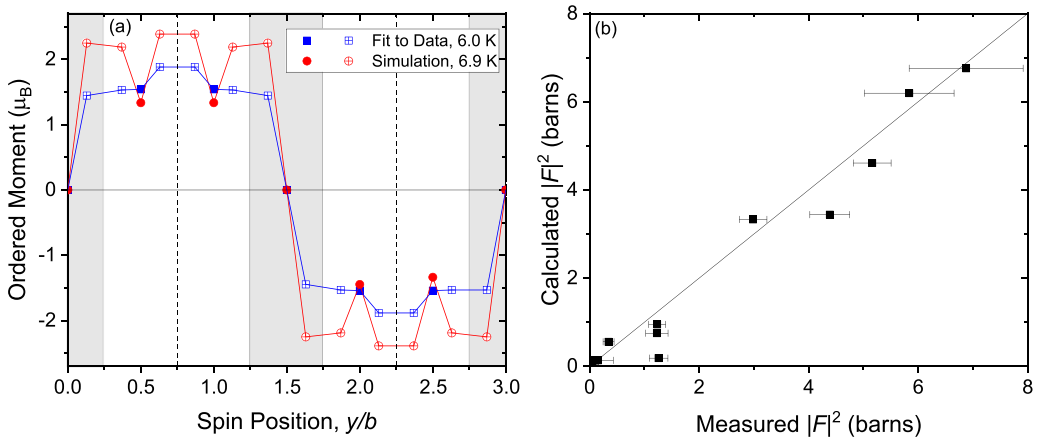

Figure 7. (a) Ordered moment along the a-axis for the $\delta = 1/3$ phase. Results are shown for the refinement of our neutron single crystal diffraction data at $T = 6.0$ K (with the cross-tie ordered moment not allowed to exceed 1.54 μ_B) and from the simulated results at $T = 6.9$ K. Cross-tie sites are shown as solid symbols, while spine sites are shown as hollow symbols with perpendicular lines. Antiferromagnetic layers are highlighted by semitransparent gray boxes, and vertical dashed lines separate the two ferromagnetic layers between each antiferromagnetic layer. (b) Comparison of the calculated (from the simulated structure) and measured (from neutron single diffraction) structure factors norm-squared for magnetic reflections.

$\delta = 1/2$ phase at 9.2 K; rather, most of the spectral weight was found in broad, heavily damped columnar excitations found at [0, 0.5, 0] reduced wave vectors. This is similar to $Ni_3V_2O_8$ [24] which also featured very broad excitations in its incommensurate phases.

The entropy of various spin density wave structures provides a natural way to describe these widths. An antiferromagnetic J_{LU} makes it energetically unfavorable for two antiferromagnetic layers to be adjacent; therefore the $\delta = 1/2$ ordered structure is nondegenerate, with alternating ferromagnetic and antiferromagnetic layers. A nondegenerate structure explains the observed resolution-limited reflection. Still, given the fact that ordered structures with different δ are very close to degenerate (assuming that $4(J_1 + J_3)S_sS_c + 4(J_5 + J_8 + 2J_{LU})S_s^2 + (2J_6 + J_{12})S_c^2 \approx 0$), we would expect fairly small ordered domains with boundaries that prevent the propagation of well-defined spin waves. A $\delta = 1/3$ ordered structure is highly degenerate assuming that all spin ordered moments are fixed. However, the stability of a $\delta = 1/3$ lock-in phase suggests that this ordered structure with two ferromagnetic layers between each antiferromagnetic layer is particularly stabilized. This leads to a resolution limited primary reflection while thermal fluctuations into the continuum of nearly degenerate states provides a broad Lorentzian component on top of this. At an incommensurate propagation vector of $\delta \approx 0.4$ the structures are highly degenerate, with sets of either one or more ferromagnetic layers in a distribution with a high degree of randomness. This leads to a reflection with a single broadened component. However, the measured width of this phase indicates some level of order. A completely random $\delta = 2/5$ phase structure was modeled with antiferromagnetic layers separated by a number of ferromagnetic layers given by one plus a random integer generated from a Poisson distribution with a mean of 0.5 (an average of 1.5 ferromagnetic layers yielding $\delta = 2/5$). This model structure produced a scattering pattern that fit to a Lorentzian with a width (FWHM) of at least 0.08 r.l.u., which is more than five times broader than the experimental observation [15]. Similar to the case of the $\delta = 1/3$ lock-in phase, the complete degeneracy of states with the same δ assumes that all spin ordered moments are fixed. Allowing for slightly different ordered moments likely favors some order, but the domains (along the b-axis) are fairly small. Both of these phases point to the fact that this model is likely overestimating the entropy, but this could be compensated by a change in the size of domains within the ac-plane as described earlier.

6. Conclusions

$Co_3V_2O_8$ features spin-3/2 Co^{2+} ions decorating a kagome staircase lattice. Previous diffraction measurements have found that, between the temperatures of 6.2 K and 11.3 K, the system displays a transversely polarized spin density wave structure with a propagation vector that evolves continuously with temperature as an incommensurate propagation vector with distinct commensurate lock-ins at both $\delta = 1/3$ and $\delta = 1/2$ [10]. It has been suggested [8] that continuously changing coupling strengths due to Co displacements could drive this behavior. While this phenomenon might play a role, we present a simple model demonstrating that this behavior could occur even with constant coupling strengths as classical thermal fluctuations select between nearly degenerate ordered structures caused by nearly balanced competing interactions. A simulation was created to determine the lowest free-energy self consistent ordered structures. Using the Hamiltonian determined from ferromagnetic spin wave measurements [18], plus two additional antiferromagnetic interactions that were suggested by a minimal Ising model [10] and were sufficiently weak as to not appreciably affect the spin wave results, the temperature dependence of the incommensurate propagation vector and commensurate

lock-ins could be semi-quantitatively modeled. A comparison of simulated magnetic structures in the $\delta = 1/2$ and $\delta = 1/3$ phases to refined structures from, respectively, previously measured [10] powder diffraction data and newly measured single crystal diffraction data revealed consistent structural motifs. When modest magnetic fields were applied along the a-axis (the magnetization easy-axis) a new $\delta = 2/5$ commensurate lock-in was stabilized, consistent with single crystal diffraction results [12]. An interesting feature of the proposed antiferromagnetic structural motif is that the energies depend upon the number of antiferromagnetic layers but generally (assuming that the number of adjacent antiferromagnetic layers is minimized) do not depend upon the location of these layers. This indicates a stacking entropy for all magnetic structures with $\delta \neq 1/2$. This entropy drives the selection of incommensurate magnetic structures by thermal fluctuations in a manner similar to an order-by-disorder mechanism in which quantum fluctuations select among degenerate ground states in strongly correlated systems [25, 26] including kagome lattice antiferromagnets [27]. The entropy of structures with $\delta \neq 1/2$ provides a mechanism to explain the broader-than-resolution peaks observed in single crystal diffraction measurements [15].

Data availability statement

All data that support the findings of this study are included within the article (and any supplementary files).

Appendix

A.1. Entropy calculation

For an isolated spin-3/2 moment in a magnetic field, the ordered spin will be given by

$$s = \sum_m p_m m = p_{-3/2}\frac{-3}{2} + p_{-1/2}\frac{-1}{2} + p_{+1/2}\frac{1}{2} + p_{+3/2}\frac{3}{2} \tag{4}$$

where p_m is the probability that a measurement of the spin angular momentum along the magnetic field direction would yield $m\hbar$ and the possible quantum numbers are $m = -\frac{3}{2}, -\frac{1}{2}, +\frac{1}{2}$, and $+\frac{3}{2}$. This probability is given by

$$p_m = \frac{1}{Z} e^{-\frac{g\mu_B m \mu_0 H}{k_B T}} \tag{5}$$

with the partition function given by

$$Z = \sum_m e^{-\frac{g\mu_B m \mu_0 H}{k_B T}}. \tag{6}$$

The entropy of this spin is given by

$$S_{\text{per spin}} = -k_B \sum_m p_m \ln(p_m). \tag{7}$$

In this way the value of the ordered spin can be directly connected with its entropy, with a fully ordered spin ($s = 3/2$) having zero entropy and a fully disordered spin ($s = 0$) having entropy $S = k_B \ln(4)$.

We should also consider the fact that (assuming that spine and cross-tie ordered moments are constant) the energy of ordered structures will depend upon the number of antiferromagnetic layers but not their locations, provided that two antiferromagnetic layers are never adjacent. This means that structures with $\delta < 1/2$ will have a stacking entropy determined by the number of equally energetic ways of arranging a particular number of antiferromagnetic layers. We will rely upon a well-known result in combinatorics [28] often called the 'stars and bars problem' which shows that the number of distinct ways of distributing n indistinguishable objects into k distinguishable bins is given by

$$\begin{pmatrix} n+k-1 \\ n \end{pmatrix} \equiv \frac{(n+k-1)!}{(n)!\,(k-1)!}. \tag{8}$$

If we further specify that each bin must contain at least one object (assuming that $n \geqslant k$) we can start by first distributing one object into each bin and then applying the previous formula to the remaining $n-k$ objects to obtain

$$\begin{pmatrix} n-1 \\ n-k \end{pmatrix} \equiv \frac{(n-1)!}{(n-k)!\,(k-1)!}. \tag{9}$$

Consider a series of N kagome layers (or $N/2$ nuclear unit cells). An ordered structure with $\delta = 1/2$ will feature $N/2$ ferromagnetic layers and $N/2$ antiferromagnetic layers. Because it is energetically unfavorable to place two antiferromagnetic layers adjacent to on another this structure is inherently nondegenerate: the only $\delta = 1/2$ magnetic structure with this energy will be the one in which ferromagnetic and antiferromagnetic layers alternate. Adding ferromagnetic layers into this has the effect of lowering δ. Suppose we add ηN ferromagnetic layers into this structure (this does not necessarily result in a net magnetic moment as there are ferromagnetic layers pointing in both directions along the a-axis). There were originally $N/2$ ferromagnetic layers serving as bins into which the ηN new ferromagnetic layers can be added. The number of distinct ways that ηN layers can be placed into $N/2$ bins is equal to

$$\Omega = \begin{pmatrix} N/2+\eta N-1 \\ \eta N \end{pmatrix} \equiv \frac{(N/2+\eta N-1)!}{(\eta N)!\;(N/2-1)!}. \tag{10}$$

By the Boltzmann formula this degenerate magnetic structure will have an entropy equal to $S = k_B \ln \Omega$. This new magnetic structure will have $N/2$ antiferromagnetic layers among $(1+\eta)N$ total layers, implying that $\delta = \frac{1}{2(1+\eta)}$. We assume that $N \gg 1$, use the Stirling approximation ($\ln N! \approx N \ln N$), divide by the number of layers, and convert from η to δ to determine that the entropy per kagome layer of a structure with $0 \leqslant \delta \leqslant 1/2$ is equal to

$$k_B\left[(1-\delta)\ln(1-\delta) - (1-2\delta)\ln(1-2\delta) - \delta\ln\delta\right]. \tag{11}$$

A.1.1. General formula for $H=0$. This entropy formula is logically easy to deduce, but applies to a very limited scenario. Now we derive generally applicable formulas to define the entropy of a magnetic structure. Consider a series of N kagome layers (or $N/2$ nuclear unit cells), each of which is either a ferromagnetic layer or an antiferromagnetic layer; it will contain δN antiferromagnetic layers and $(1-\delta)N$ ferromagnetic layers. The δN antiferromagnetic layers are grouped into χN 'sets' of one or more consecutive layers. Between each set of antiferromagnetic layers there will be at least one ferromagnetic layer. Clearly, $\chi \leqslant \delta$; when $\delta > 1/2$ it becomes necessary that some antiferromagnetic layers are placed adjacent in the same set and $\chi \leqslant (1-\delta)$. Because it is energetically unfavorable to place two antiferromagnetic layers adjacent, the lowest energy state for a given δ will occur when χ is as large as possible. We will start by considering the case where the applied magnetic field is zero, so there is no energy dependence upon the relative number of ferromagnetic layers pointing in each direction. First we place one antiferromagnetic layer into each set. Then we determine the number of distinct ways of placing the remaining $(\delta-\chi)N$ antiferromagnetic layers into the χN sets. This is

$$\Omega_1 = \begin{pmatrix} \delta N-1 \\ (\delta-\chi)N \end{pmatrix} \equiv \frac{(\delta N-1)!}{((\delta-\chi)N)!\ (\chi N-1)!}. \quad (12)$$

We then need to place the $(1-\delta)N$ ferromagnetic layers into χN sets: each set of antiferromagnetic layers is directly followed by a set of ferromagnetic layers, so the number of sets must be equal. Again, there must be a minimum of one layer in each set. Similarly, the number of ways of doing this is

$$\Omega_2 = \begin{pmatrix} (1-\delta)N-1 \\ (1-\delta-\chi)N \end{pmatrix} \equiv \frac{((1-\delta)N-1)!}{((1-\delta-\chi)N)!\ (\chi N-1)!}. \quad (13)$$

The total degeneracy of this state is the product of these two individual degeneracies:

$$\Omega = \frac{(\delta N-1)!\,((1-\delta)N-1)!}{((\delta-\chi)N)!\,((1-\delta-\chi)N!\,((\chi N-1)!)^2}. \quad (14)$$

From this we find that the entropy per kagome layer is equal to

$$k_B[\delta\ln\delta + (1-\delta)\ln(1-\delta) - (\delta-\chi)\ln(\delta-\chi) - (1-\delta-\chi)\ln(1-\delta-\chi) - 2\chi\ln\chi]. \quad (15)$$

Note that this equation reproduces equation (11) when $\chi=\delta$, which will be true for the most energetically favorable structure at a given δ with $0 \leqslant \delta \leqslant 1/2$.

A.1.2. General formula for $H>0$. When there is an applied magnetic field along the a-axis the degeneracy between magnetic structures with different numbers of ferromagnetic layers pointing in each direction is lifted. Again, we will consider δN antiferromagnetic layers and $(1-\delta)N$ ferromagnetic layers each split into χN sets. But now we further state that the ferromagnetic layers consist of ηN layers pointing up grouped into ϕN sets and $(1-\delta-\eta)N$ layers pointing down grouped into $(\chi-\phi)N$ sets. When the antiferromagnetic set between two ferromagnetic sets contains an odd number of antiferromagnetic layers the two ferromagnetic sets will point in opposite directions, while if it contains an even number of antiferromagnetic layers the two ferromagnetic sets will point in the same direction. We will assume without loss of generality that $\phi \geqslant \chi/2$: we are defining 'up' to be the direction that has more ferromagnetic sets.

We start off by taking $2\phi N$ antiferromagnetic layers and using them to created $2\phi N$ antiferromagnetic sets each containing one layer. This leaves ϕN spaces for ferromagnetic sets pointing up and ϕN spaces for ferromagnetic sets pointing down. However, we will have only $(\chi-\phi)N$ sets pointing down. This means that $(2\phi-\chi)N$ of the sets set aside for ferromagnetic sets pointing down will be left empty. If a place for a ferromagnetic set pointing down is left empty, the antiferromagnetic sets on each side (both of which contain one layer) merge to form a single antiferromagnetic set with two layers that is placed between two ferromagnetic sets both pointing up. The number of distinct ways of choosing which spots are left empty is

$$\Omega_1 = \begin{pmatrix} \phi N \\ (2\phi-\chi)N \end{pmatrix} \equiv \frac{(\phi N)!}{((2\phi-\chi)N)!\ ((\chi-\phi)N)!}. \quad (16)$$

There are now $(\delta-2\phi)N$ antiferromagnetic layers remaining. The number of antiferromagnetic sets is now χN. We need to distribute the $(\delta-2\phi)N$ layers into the χN sets, but it must be done in groups of two so that the number of antiferromagnetic sets containing an even number of layers remains constant. This is equivalent to the number of ways of distributing $(\delta/2-\phi)N$ elements into χN sets. This is

$$\Omega_2 = \begin{pmatrix} (\delta/2-\phi+\chi)N-1 \\ (\delta/2-\phi)N \end{pmatrix} \equiv \frac{(\delta/2-\phi+\chi)N-1)!}{((\delta/2-\phi)N)!\ (\chi N-1)!}. \quad (17)$$

Third, we then determine the number of distinct ways to place ηN ferromagnetic layers pointing up into the ϕN places for them, again requiring that there be at least one layer per set. This is

$$\Omega_3 = \begin{pmatrix} \eta N-1 \\ (\eta-\phi)N \end{pmatrix} \equiv \frac{(\eta N-1)!}{((\eta-\phi)N)!\ (\phi N-1)!}. \quad (18)$$

Finally, we need to determine the number of ways of placing the $(1-\delta-\eta)N$ ferromagnetic layers pointing down into the $(\chi-\phi)N$ spots remaining for them, with the constraint that there is at least one layer in each spot. The number of ways of doing this is

$$\Omega_4 = \begin{pmatrix} (1-\delta-\eta)N-1 \\ (1-\delta-\eta-\chi+\phi)N \end{pmatrix} \equiv \frac{((1-\delta-\eta)N-1)!}{((1-\delta-\eta-\chi+\phi)N)!\ ((\chi-\phi)N-1)!}. \quad (19)$$

Multiplying these four degeneracies in order to determine the total degeneracy, we find an entropy per layer of

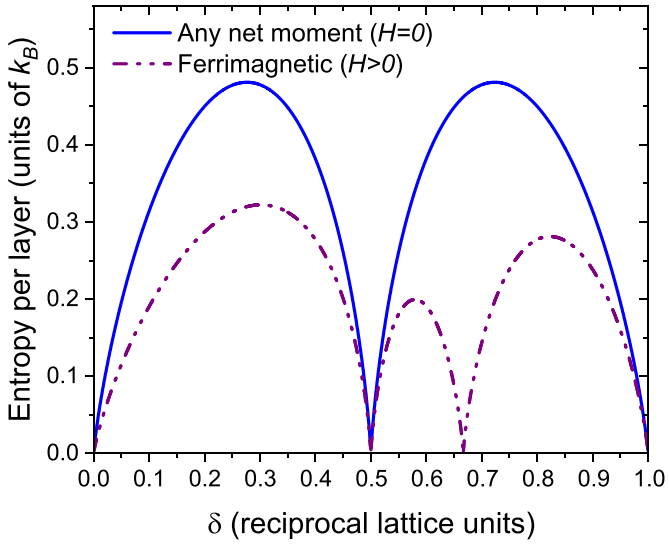

Figure 8. The calculated entropy per layer of magnetic structures is plotted as a function of the propagation vector component δ. The entropy of all structures (with any net magnetic moment) is shown as the solid line; this entropy is the appropriate description when there is no magnetic field. The entropy of structures that feature the maximum possible ferrimagnetic moment for that δ is shown as the dashed line; this entropy is used when the applied magnetic field is nonzero so that the energy will depend upon the net moment.

$$\begin{aligned} k_B[&(\delta/2-\phi+\chi)\ln(\delta/2-\phi+\chi)+\eta\ln\eta \\ &+(1-\delta-\eta)\ln(1-\delta-\eta)-(2\phi-\chi)\ln(2\phi-\chi) \\ &-(\delta/2-\phi)\ln(\delta/2-\phi)-\chi\ln(\chi)-(\eta-\phi)\ln(\eta-\phi) \\ &-(1-\delta-\eta-\chi+\phi)\ln(1-\delta-\eta-\chi+\phi) \\ &-2(\chi-\phi)\ln(\chi-\phi)]. \end{aligned} \tag{20}$$

The four degeneracies derived for when $H \neq 0$ all feature the variable ϕ, where ϕN is the number of sets of ferromagnetic layers pointing up. However, the energy of the magnetic structure will be independent of ϕ: the energy will depend on the number of ferromagnetic layers pointing up and down (because $H > 0$) and the total number of sets of ferromagnetic layers (because that is related to the number of antiferromagnetic layers adjacent to another antiferromagnetic layer) but the energy is independent of how many of the ferromagnet sets are pointing up. Therefore, in order to determine the full degeneracy one would need to sum over all possible values of ϕ. Our model is therefore underestimating the entropy of individual magnetic structures in field by simply applying equation (20) using the value of ϕ presented by the structure. However, it is reasonable to think that ordered structures that minimize the free energy are likely to be those that minimize the energy for their given value of δ by maximizing the net ferrimagnetic moment. Those states have specific values of ϕ (for example, $\phi = \delta/2$ for $\delta \leqslant 1/2$) so there is no need to sum over other values of ϕ.

Figure 8 shows the entropy per kagome layer for magnetic structures as a function of the propagation vector component δ. In zero applied field structures with any net magnetic moment can still be degenerate, so that the entropy depends only on δ and χ (equation (15)). The lowest energy state for a given δ will occur when the number of adjacent antiferromagnetic layers is minimized; this occurs when χ is as large as possible for the given δ, or $\chi = \delta$ for $\delta \leqslant 1/2$ and $\chi = 1-\delta$ for $\delta \geqslant 1/2$. This entropy is shown as the solid line. When the applied magnetic field is nonzero the energy will depend on the net magnetic moment and the entropy depends on δ, χ, ϕ, and η (equation (20)). The lowest energy state will occur when the net magnetic moment is as large as possible, so that χ, η, and ϕ will be as large as possible for the given δ. This entropy is shown as the dashed line.

A.2. Diffraction data

Single crystal diffraction data were measured using the BT-4 thermal triple axis spectrometer at temperatures of 3 K, 6 K, and 15 K. A total of 21 reciprocal space positions in the $[H\,K\,0]$ scattering plane were measured. The $[H\,K\,0]$ scattering plane allows for measurement of both the primary and secondary antiferromagnetic reflections in the $\delta = 1/3$ phase; further, the weakening of intensity as $\vec{Q}$ moves away from the b-axis confirms that moments are ordered along the a-axis in this phase. Rocking scans (along θ) for a selection of positions are displayed in the following figures.

In the $\delta = 1/3$ phase strong magnetic reflections are observed at $[H, K, 0]$ positions where H is an even integer and K is an even integer $\pm 1/3$. Polarized diffraction measurements [10] suggest that this scattering is not completely magnetic in origin but contains a weak nuclear component. Figure 9 displays rocking scans measured at [0, 2.33, 0] and [2, 4.33, 0]. The intensities are quite strong at 6 K (in the $\delta = 1/3$ phase) and there is no intensity at 3 K (in the ferromagnetic phase).

In the $\delta = 1/3$ phase magnetic reflections are also observed at $[H, K, 0]$ positions where H is an even integer and K is an odd integer. These peaks represent higher-order scattering for

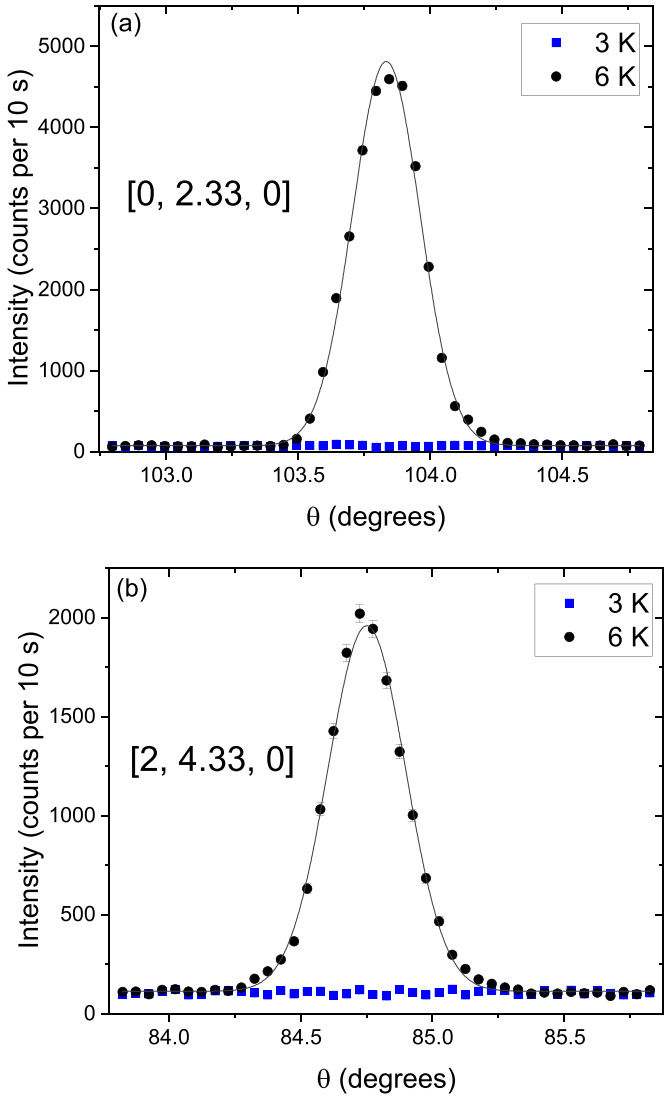

Figure 9. (a) Rocking curve through the [0, 2.33, 0] position. (b) Rocking curve through the [2, 4.33, 0] position. Lines are Gaussian fits.

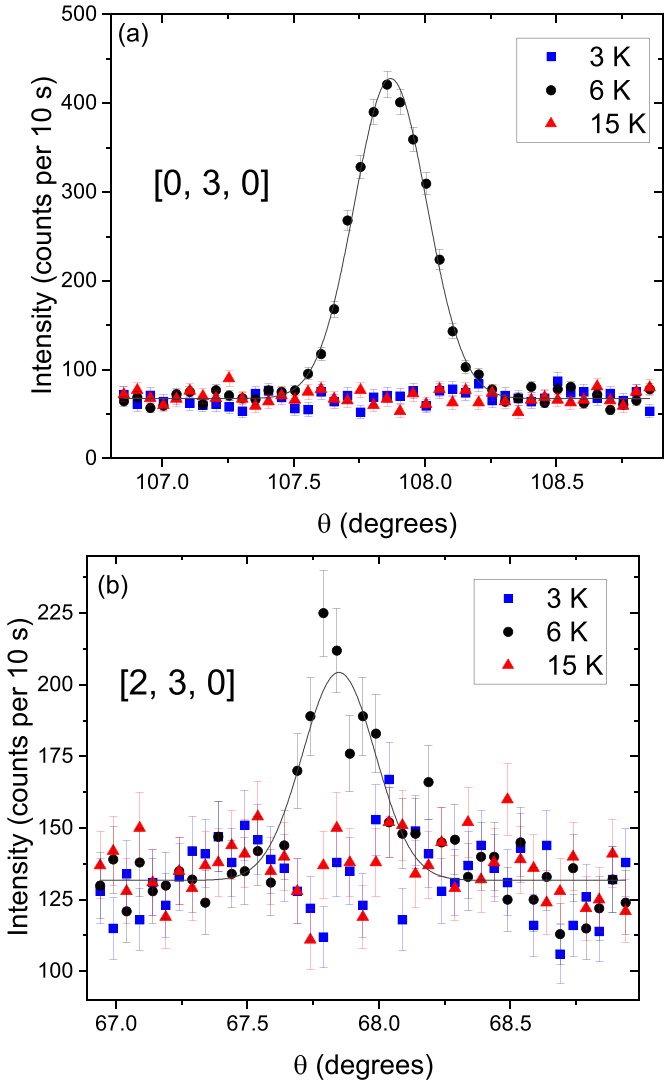

Figure 10. (a) Rocking curve through the [0, 3, 0] position. (b) Rocking curve through the [2, 3, 0] position. Lines are Gaussian fits.

$\delta = 1/3$ as higher-order reflections were observed at $\delta' = 2 - 3\delta$ [10]. Figure 10 displays rocking scans measured at [0, 3, 0] and [2, 3, 0]. Intensity is observed only at 6 K (in the $\delta = 1/3$ phase). No intensity was observed either at 3 K (in the ferromagnetic phase) or at 15 K (in the paramagnetic phase). The reflection at [2, 3, 0] is significantly weaker because the component of the spin perpendicular to $\vec{Q}$ is considerably smaller, consistent with moments ordered along the a-axis.

In the ferromagnetic phase magnetic reflections are observed at $[H, K, 0]$ positions where H and K are both even integers. Figure 11 displays rocking scans measured at [0, 4, 0] and [2, 2, 0]. Both reflections show strong intensity at 3 K, in the ferromagnetic phase. These positions also feature relatively weak nuclear Bragg peaks, so there is some intensity at both 6 K and 15 K. The difference in intensities at 3 K and 15 K was used to determine the strength of the ferromagnetic Bragg peaks. These ferromagnetic Bragg peak intensities and the intensities of nuclear Bragg peaks were used to normalize the intensities measured in the $\delta = 1/3$ phase. The intensity difference between 6 K and 15 K represents the measured intensity of magnetic reflections at these positions in the $\delta = 1/3$ phase; the measured difference between 6 K and 15 K is consistent with zero, indicating that $[H, K, 0]$ positions where H and K are both even integers do not feature any magnetic intensity in the $\delta = 1/3$ phase.

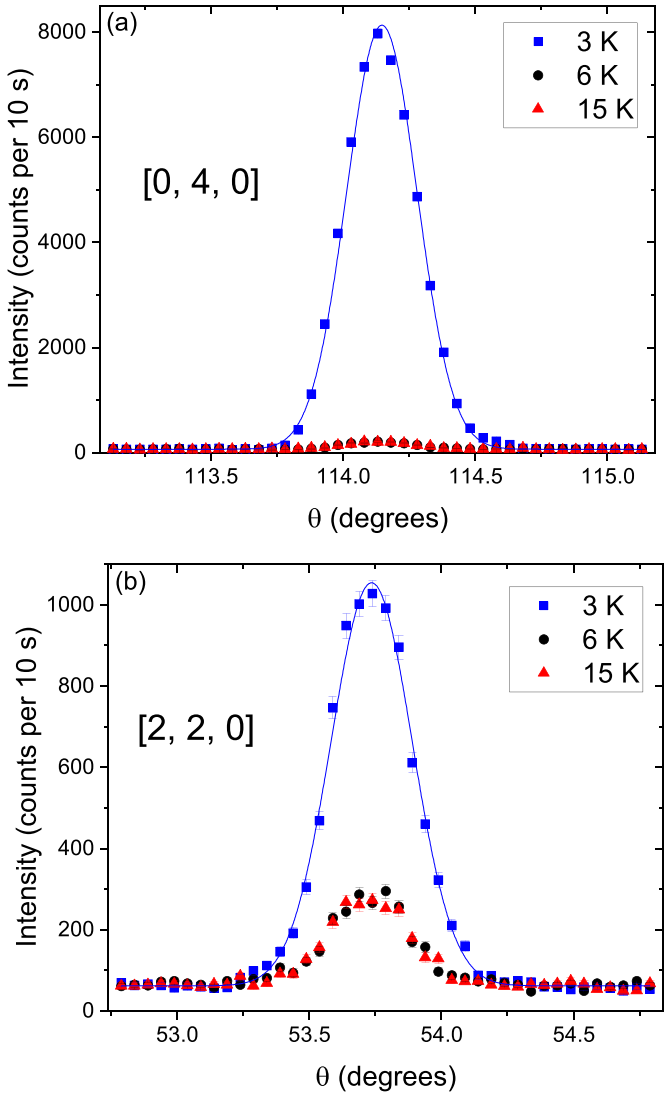

Figure 11. (a) Rocking curve through the [0, 4, 0] position. (b) Rocking curve through the [2, 4, 0] position. Lines are Gaussian fits.

ORCID iDs

Joel S Helton https://orcid.org/0000-0002-5511-2849
Jeffrey W Lynn https://orcid.org/0000-0003-3626-4932

References

[1] Ramirez A P 1994 Strongly geometrically frustrated magnets *Annu. Rev. Mater. Sci.* **24** 453–80
[2] Balents L 2010 Spin liquids in frustrated magnets *Nature* **464** 199–208
[3] Lawes G *et al* 2004 Competing magnetic phases on a Kagomé staircase *Phys. Rev. Lett.* **93** 247201
[4] Kenzelmann M *et al* 2006 Field dependence of magnetic ordering in Kagomé-staircase compound $Ni_3V_2O_8$ *Phys. Rev.* B **74** 014429
[5] Lawes G *et al* 2005 Magnetically driven ferroelectric order in $Ni_3V_2O_8$ *Phys. Rev. Lett.* **95** 087205
[6] Cabrera I *et al* 2009 Coupled magnetic and ferroelectric domains in multiferroic $Ni_3V_2O_8$ *Phys. Rev. Lett.* **103** 087201
[7] Dong C *et al* 2022 Reentrant ferroelectric phase induced by a tilting high magnetic field in $Ni_3V_2O_8$ *Phys. Rev.* B **105** 024427
[8] Vergara L I, Cao J, Tung L-C, Rogado N, Yen F, Wang Y Q, Cava R J, Lorenz B, Wang Y-J and Musfeldt J L 2010 Magnetoelastic coupling in magnetically frustrated $Co_3V_2O_8$ *Phys. Rev.* B **81** 012403
[9] Bellido N, Martin C, Simon C and Maignan A 2007 Coupled negative magnetocapacitance and magnetic susceptibility in a Kagomé staircase-like compound $Co_3V_2O_8$ *J. Phys.: Condens. Matter* **19** 056001
[10] Chen Y *et al* 2006 Complex magnetic order in the kagomé staircase compound $Co_3V_2O_8$ *Phys. Rev.* B **74** 014430
[11] Qureshi N *et al* 2009 Experimental magnetic form factors in $Co_3V_2O_8$: a combined study of *ab initio* calculations, magnetic Compton scattering and polarized neutron diffraction *Phys. Rev.* B **79** 094417
[12] Helton J S, Chen Y, Bychkov G L, Barilo S N, Rogado N, Cava R J and Lynn J W 2012 Evolution of the commensurate and incommensurate magnetic phases of the $S = 3/2$ kagome staircase $Co_3V_2O_8$ in an applied field *J. Phys.: Condens. Matter* **24** 016003
[13] Fritsch K, Ehlers G, Rule K C, Habicht K, Ramazanoglu M, Dabkowska H A and Gaulin B D 2015 Quantum phase transitions and decoupling of magnetic sublattices in the quasi-two-dimensional Ising magnet $Co_3V_2O_8$ in a transverse magnetic field *Phys. Rev.* B **92** 180404(R)
[14] Yasui Y, Kobayashi Y, Soda M, Moyoshi T, Sato M, Igawa N and Kakurai K 2007 Successive magnetic transitions of the kagomé staircase compound $Co_3V_2O_8$ studied in various magnetic fields *J. Phys. Soc. Japan* **76** 034706
[15] Petrenko O A, Wilson N R, Balakrishnan G, Paul D M and McIntyre G J 2010 Kagome staircase compound $Co_3V_2O_8$ in an applied magnetic field: single-crystal neutron diffraction study *Phys. Rev.* B **82** 104409
[16] Zhao X, Wu J C, Zhao Z Y, He Z Z, Song J D, Zhao J Y, Liu X G, Sun X F and Li X G 2016 Heat switch effect in an antiferromagnetic insulator $Co_3V_2O_8$ *Appl. Phys. Lett.* **108** 242405
[17] Ramazanoglu M, Adams C P, Clancy J P, Berlinsky A J, Yamani Z, Szymczak R, Szymczak H, Fink-Finowicki J and Gaulin B D 2009 Spin waves in the ferromagnetic ground state of the kagome staircase system $Co_3V_2O_8$ *Phys. Rev.* B **79** 024417
[18] Helton J S, Butch N, Pajerowski D, Barilo S N and Lynn J W 2020 Three-dimensional magnetism and the Dzyaloshinskii-Moriya interaction in $S = 3/2$ kagome staircase $Co_3V_2O_8$ *Sci. Adv.* **6** aay9709
[19] Wilson N R, Petrenko O A, Balakrishnan G, Manuel P and Fåk B 2007 Magnetic excitations in the kagome staircase compounds *J. Magn. Magn. Mater.* **310** 1334–6
[20] Rogado N, Lawes G, Huse D A, Ramirez A P and Cava R J 2002 The Kagomé-staircase lattice: magnetic ordering in $Ni_3V_2O_8$ and $Co_3V_2O_8$ *Solid State Commun.* **124** 229–33
[21] Momma K and Izumi F 2011 VESTA 3 for three-dimensional visualization of crystal, volumetric and morphology data *J. Appl. Crystallogr.* **44** 1272–6

[22] Weiss P 1907 L'hypothèse du champ moléculaire et la propriété ferromagnétique *J. Phys. Theor. Appl.* **6** 661
[23] Toth S and Lake B 2015 Linear spin wave theory for single-q incommensurate magnetic structures *J. Phys.: Condens. Matter* **27** 166002
[24] Ehlers G, Podlesnyak A A, Frontzek M D, Pushkarev A V, Shiryaev S V and Barilo S 2015 Damped spin waves in the intermediate ordered phases in $Ni_3V_2O_8$ *J. Phys.: Condens. Matter* **27** 256003
[25] Villain J, Bidaux R, Carton J-P and Conte R 1980 Order as an effect of disorder *J. Phys. France* **41** 1263–72
[26] Bergman D, Alicea J, Gull E, Trebst S and Balents L 2007 Order-by-disorder and spiral spin-liquid in frustrated diamond-lattice antiferromagnets *Nat. Phys.* **3** 487–91
[27] Chubukov A 1992 Order from disorder in a kagomé antiferromagnet *Phys. Rev. Lett.* **69** 832–5
[28] Ehrenfest P and Kamerlingh Onnes H 1915 Simplified deduction of the formula from the theory of combinations which Planck uses as the basis of his radiation theory *London, Edinburgh Dublin Phil. Mag. J. Sci.* **6** 297–301